

## Article

# Modeling and Optimizing the Performance of Green Forage Maize Harvester Header Using a Combined Response Surface Methodology–Artificial Neural Network Approach

Zhao Xue <sup>1,2</sup>, Jun Fu <sup>1,2</sup>, Qiankun Fu <sup>1,2,\*</sup>, Xiaokang Li <sup>3</sup> and Zhi Chen <sup>4</sup>

<sup>1</sup> College of Biological and Agricultural Engineering, Jilin University, Changchun 130022, China; xuez20@mails.jlu.edu.cn (Z.X.); fu\_jun@jlu.edu.cn (J.F.)

<sup>2</sup> Key Laboratory of Efficient Sowing and Harvesting Equipment, Ministry of Agriculture and Rural Affairs, Jilin University, Changchun 130022, China

<sup>3</sup> Gansu Academy of Mechanical Sciences Co., Ltd., Lanzhou 730030, China; xiaokang\_li01@163.com

<sup>4</sup> Chinese Academy of Agricultural Mechanization Sciences, Beijing 100083, China; chenzhi@caamm.org.cn

\* Correspondence: qkfu@jlu.edu.cn

**Abstract:** Green forage maize harvesters face challenges such as high soil humidity and soft soil in the field, mismatched working parameters, and poor reliability and adaptability. These challenges often result in header blockage, significant harvest loss, and increased energy consumption. Traditional testing and statistical analysis methods used in most existing studies are limited by complex test processes, their time-consuming nature, high costs, and poor prediction accuracy. To address these problems, a test bench was constructed to analyze the effects of forward speed, cutting height, number of rows, and their interactions on specific energy consumption and harvest loss of the green forage maize (GFM) header. A combined response surface method (RSM)–artificial neural network (ANN) approach is proposed for modeling and predicting the performance parameters of the header. The optimal conditions were determined by optimizing the specific energy consumption and loss rate. The optimal combination parameters are a forward speed of 1.6 km/h, a cutting height of 167 mm, and a number of rows of 4. However, RSM–ANN has larger  $R^2$  values and lower root mean square errors (RMSE) and mean square errors (MSE) compared to RSM. Specifically, the  $R^2$  of the RSM–ANN model for specific energy consumption and loss rate a 0.9925 and 0.9906, MSE are 0.00001775 and 0.004558, and RMSE are 0.004214 and 0.006752, respectively. The results show that the combined RSM–ANN method has higher precision and accuracy and can better predict and optimize the header performance. This study overcomes the limitations of traditional methods and has the potential to provide data and method references for the design, optimization, prediction, and intelligent diagnosis of faults in the operational parameters of agricultural machinery.

**Keywords:** green forage maize; harvest; specific energy consumption; response surface methodology (RSM); artificial neural network (ANN)



**Citation:** Xue, Z.; Fu, J.; Fu, Q.; Li, X.; Chen, Z. Modeling and Optimizing the Performance of Green Forage Maize Harvester Header Using a Combined Response Surface Methodology–Artificial Neural Network Approach. *Agriculture* **2023**, *13*, 1890. <https://doi.org/10.3390/agriculture13101890>

Academic Editors: Ning Wang, Changyuan Zhai and Jianfeng Zhou

Received: 21 August 2023

Revised: 18 September 2023

Accepted: 25 September 2023

Published: 27 September 2023



**Copyright:** © 2023 by the authors. Licensee MDPI, Basel, Switzerland. This article is an open access article distributed under the terms and conditions of the Creative Commons Attribution (CC BY) license (<https://creativecommons.org/licenses/by/4.0/>).

## 1. Introduction

In recent years, maize production has increased dramatically in line with the growing population's demand for food [1,2]. At the same time, a large amount of agricultural waste (maize stalk) is produced, which is considered to be the most abundant biomass resource [3]. Approximately 264 million tons of maize stalks are produced annually in China, and most of them are discarded or burned directly in the field [4]. Direct combustion can produce greenhouse gases (such as carbon dioxide), particulate matter, and other pollutants, which affect the atmospheric environment and ecosystem [5]. On the other hand, it can cause waste of energy [6]. Green forage maize (GFM) (*Zea mays* L.) is an important feed source for the world's developed animal husbandry countries because of its high yield and nutrient content and is well suited to solve the problem of maize stalk utilization.

In addition, utilizing maize stalks as animal feed can reduce environmental burdens, promote the development of animal-derived foods, increase incomes, and improve social sustainability [7]. China's GFM has grown rapidly in recent years under the guidance of the 'Grain to Feed' policy. At present, forage harvesters are widely used in GFM harvesting to ensure high harvest yield and quality and reduce labor intensity. However, the use of harvesters requires the consumption of fossil fuels and the emission of greenhouse gases, which can pose a threat to the environment and social sustainability [8,9]. Due to the high soil moisture in the field and the mismatch of operation parameters during the harvest of GFM, it is easy to cause header blockage, leading to increased fossil fuel consumption, pollutant emissions, and biomass energy loss. Therefore, it is of practical significance to reduce the environmental burden and save energy by optimizing the harvesting process of GFM harvesters to reduce energy consumption and increase efficiency.

The header, which is the first contact with crops, is the key component of a forage harvester. It is responsible for cutting and feeding the crops. Cutting is one of the most energy-intensive parts of harvesting [10]. Compared with foreign countries, most of the existing machines in China are designed via empirical methods, and there are some problems such as poor adaptability and mismatch of operation parameters [11,12]. This results in the stalks not being cut off and smoothly fed into the harvester, seriously affecting the quality of the harvest. In addition, the fallen stalk may block the header, resulting in increased energy consumption and pollutant emissions. Scholars at home and abroad have conducted numerous studies on header technology, mainly focusing on theoretical analysis of cutting [13–15], overall design and testing of headers [16–18], and the design and optimization of key components [19]. However, there have been few reports on the interaction between GFM and header, operation parameter matching, and header performance optimization. Notably, the structural parameters (cutter form, cutting method, etc.), movement parameters (cutting speed, forward speed, etc.), and crop parameters (stalk diameter, plant spacing, row spacing, etc.) independently or jointly affect the performance of the header. However, it is complex, time-consuming and expensive to study the influence of various factors on header performance and to analyze optimal parameter conditions via traditional methods (one-factor-at-a-time approach). Furthermore, the method does not take into account the interactions between factors and cannot obtain true optimal conditions [20,21]. To address these issues, empirical models for parameter optimization and modeling should be developed using state-of-the-art statistical methods or data analysis tools, and the independent or joint effects of these factors on the response should be analyzed.

Response surface methodology (RSM) is an advanced mathematical and statistical tool used to evaluate the relationship between the output responses and the multiple independent input variables. It can also optimize these variables to achieve the best responses [22]. Box–Behnken design (BBD) is one of the most commonly used methods of RSM. It allows for the study of the influence of multiple variables and their interactions on the response by changing these variables simultaneously and conducting fewer experiments [23]. However, RSM has limitations on the range of input variables due to its nonlinear process [24]. Conversely, the artificial neural network (ANN) is a highly robust and excellent modeling tool generally used in nonlinear and complex processes, which can effectively overcome the limitations of RSM [25]. At present, ANN and RSM have been widely used in structural design optimization of agricultural machinery [26], design optimization of food processing machinery [27], food process optimization [28], and industrial process optimization [29,30]. In fact, GFM harvesting is a complex process, affected by many factors, and conducting trials requires a great deal of time and high costs. The RSM method can be used to run relatively few experiments [27]. However, its prediction ability still needs to be further tested. Compared to RSM, ANN is more widely used in forecasting and has relatively good forecasting ability [28]. However, the feasibility of using artificial intelligence technologies such as RSM and ANN in combination to predict and optimize the performance of the header for green forage maize harvesters has not been fully investigated.

To solve the above problems, a GFM harvesting test bench was built, and the effect of various factors on header performance, especially on energy consumption and harvest loss, was studied. In addition, a combined RSM–ANN method is proposed, which can simultaneously complete interaction analysis and performance optimization and guarantee high prediction accuracy. The main objectives of this study are as follows: (1) To determine the optimized operating parameters of the header of the GFM harvester; (2) To analyze the influence of each factor and its interaction on loss rate and specific energy consumption; (3) To develop the predicting models for the header performance of the GFM harvester. This study overcomes the limitations of traditional methods and can provide data and method references for the design, optimization, prediction, and intelligent fault diagnosis of the operation parameters of agricultural machinery.

## 2. Materials and Methods

In this section, we first introduce the harvesting process of the GFM. Then we describe the test bench and test control system and its working principle. Next, we introduce the materials used in this study. Finally, we introduce the methods of experiment design, statistical analysis, and artificial neural network.

### 2.1. Harvesting Process of Green Forage Maize

A crawler GFM harvester consists of the crawler chassis, cab, header, throwing device, chopping device, and other parts. It is suitable for GFM harvesting in areas with high humidity, soft soil, varied topography and geomorphology, and complex operating conditions and can effectively solve the problems of high soil compaction, failure to operate in wet fields, and discontinuous operation in complex plots of wheel harvesters. The header, the key part of the green forage maize harvester, is the first contact with the crop, which is related to the structure and parameter configuration and the working performance of the whole machine, so it directly affects the adaptability of the harvester to the terrain, geomorphology, and planting agronomy. The header is mainly composed of the divider, push rod, conveying drum, conveying teeth, and cutter, as shown in Figure 1.

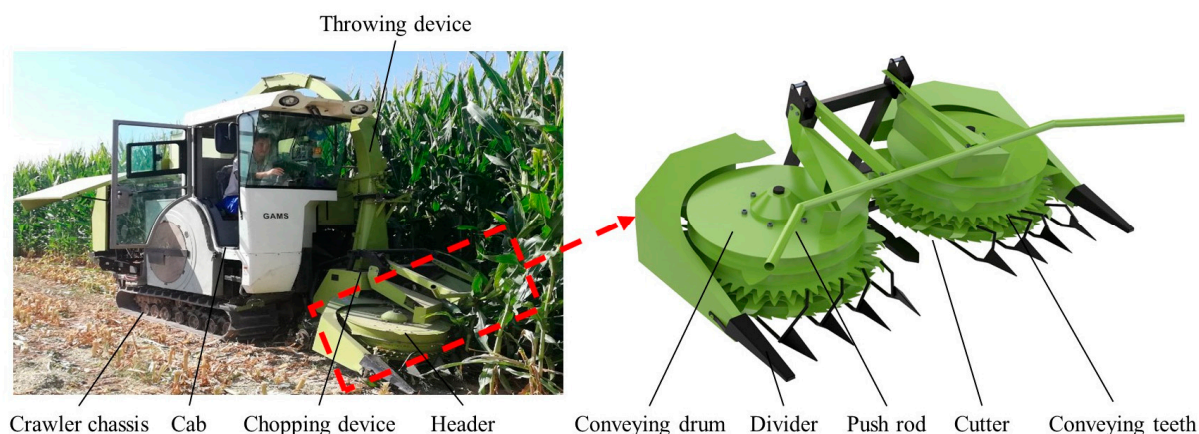


**Figure 1.** Harvesting process and harvester header structure of green forage maize.

During the harvesting process, the operator controls the harvester's forward motion to ensure that the stalks reach the header smoothly through the divider to complete the cutting operation. However, the operator usually relies on experience to gauge the forward speed of the harvester and cutting height of the header, which can easily break the stalk and cause harvest loss. The uncut stalk is likely to wrap around the header, resulting in blockage and increased energy consumption. The number of stalk planting rows directly determines the planting density, which affects the harvest quality and effect of the header. The more rows, the more stalks cut and fed by the header, and the specific energy consumption of the header increases. Additionally, an increase in the stalk interaction can affect the smooth feeding of stalks, increasing the risk of header block, and the loss rate of the header.

Therefore, we focus on the impact of forward speed, cutting height, and number of rows on the specific energy consumption and loss rate of the header.

## 2.2. Test Bench and Test Control System

Aiming at the problems of complex, time-consuming, expensive field experiments, difficult data acquisition, and low parameter control accuracy, this study designed a GFM harvesting test bench to simulate the field harvesting process of crawler harvesters, and carried out the header performance tests.

The harvesting test bench consists of a frame, power input device, throwing device, chopping device, feeding device, header, material conveyor, and test control system, as shown in Figure 1. Among them, the header suspended at the front of the frame via the three-point suspension mechanism is one of the key components of the bench. It consists mainly of dividers, a push rod, header drums, conveying teeth, and cutters. In order to ensure that the test is approximately consistent with the actual operation process, we tilted the header by 8 degrees [31]. In addition, we installed the feeding device and the chopping device at the rear of the header to achieve feeding and chopping. The power input device is located on the rear right side of the header and is fixed to the frame. It is composed of a variable frequency motor, coupling, and torque-speed sensor, and transmits power to the header through the variable frequency motor. The material conveyor is at the front of the header and extends its end to the bottom of the cutter, which is driven by a variable frequency motor. We also set an adjustable clamping mechanism on the surface of the conveyor chain plate to fix the materials and realize the simulation of the real growth state of field crops. The principle of this test bench is the same as that of crawler GFM harvesters used in hilly and mountainous areas, which can completely simulate the actual harvesting process and carry out the performance test of the header. The relevant parameters of the test bench are shown in Table 1.

**Table 1.** Parameters of test bench.

Parameters	Value
Size (length × width × height) (mm × mm × mm)	7700 × 2750 × 4050
Forward speed/(m·s <sup>-1</sup> )	≥0.5
Cutting length/mm	11~29
Power/kW	80
Working width/mm	1800
Disc cutter diameter/mm	738
Cutter speed/(r/min)	1106
Drum speed/(r/min)	36.6
Cutter blade thickness/mm	3
Serrated blade edge length/mm	6
Serrated blade edge angle/°	65

The test control system is mainly composed of a human-machine interface (HMI) (MCGS, model: TCP1062K), a programmable logic controller (PLC) (DELTA, model: DVP12SA211T), a torque-speed sensor (Haibohua, model: HCNJ-101), a wireless transparent transmission module (EBYTE, model: E90-DTU), a frequency converter (INVT, GD200A-022G/03P-4), and a motor, as shown in Figure 2. The torque-speed sensor is between the motor and the header and has a measurement range of 0 to 2000 Nm with an accuracy of ±0.5%. The signal conversion module converts the torque frequency signal and the speed pulse signal of the sensor into a digital signal and transmits the signal to PLC. Moreover, the HMI can control the frequency converter to change the speed of the motor, display the running state, and monitor the parameters of the equipment in real time. The software then reads the data processed by the PLC and performs visual processing, and the wireless communication module transmits the relevant data to the database.

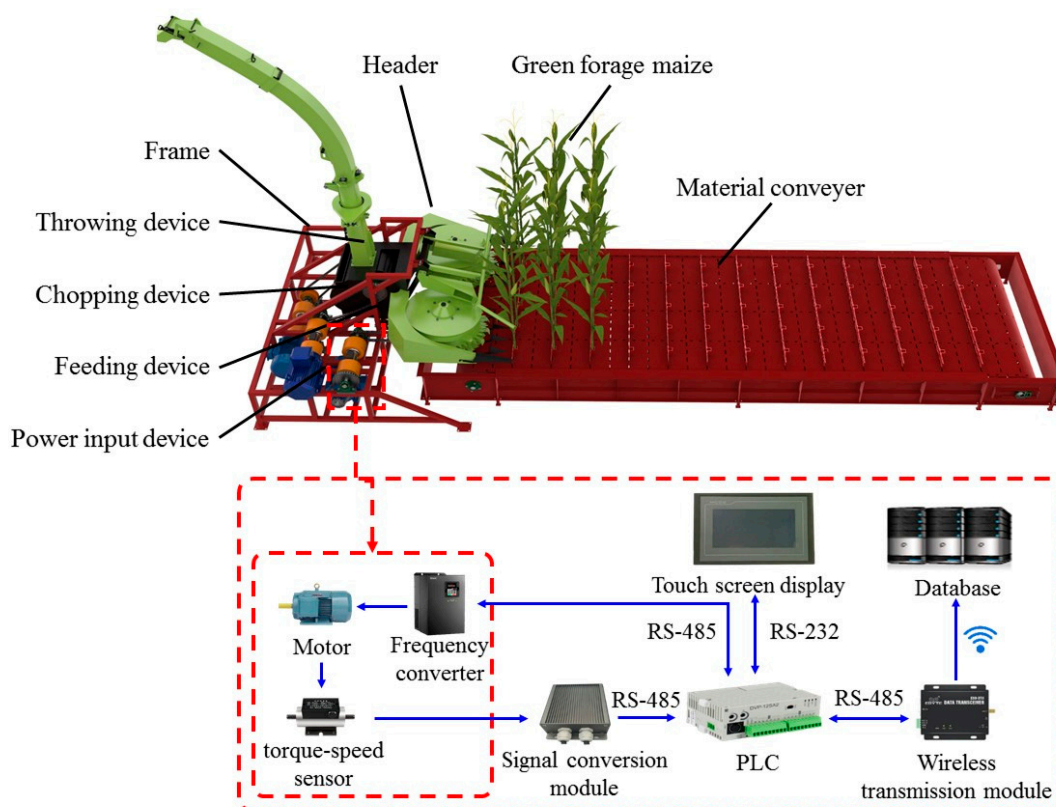


**Figure 2.** Structure of test bench and test control system.

### 2.3. Working Principle

The conveyor transports the materials to the header and completes the harvest operation to simulate the actual harvest process of the crawler GFM harvester in the field in hilly and mountainous areas. Before the test, the whole-plant GFM is fixed on the conveyor with the clamping mechanism. At the same time, we can change the row spacing, plant spacing, and cutting height by adjusting the clamping mechanism. Due to the high humidity of the field during harvest, especially in hilly and mountainous areas, the ground level is uneven, resulting in the low operating speed of the GFM harvester. Hence, to simulate the field operation speed of the crawler harvester, we can use the adjustable motor to adjust the speed range from 0 to 2.5 km/h. The sprocket and other transmission mechanisms transmit the power to the header, feeding device, and chopping device, and the control system can change the forward speed. During the test, the divider guides the materials into the header and the cutter at the bottom of the header cuts along the cutting height of the stalk. Consequently, the cut stalk is transported backward under the action of the rotation of the header drum, and the crop is transported to the chopping device via the feeding device to complete the chopping and throwing operation. In this process, the test control system can monitor torque and speed information via the torque-speed sensor in real time and collect, record, and process the relevant test data.

### 2.4. Material Selection

In this study, the GFM of Wuke silage 107 was selected, which is harvested in the experimental field of Huangyang Town, Wuwei City, Gansu Province in mid-September 2020 (at the wax ripening stage of green forage maize in Northwest China, which is the best time for harvest). Before the test, we used Vernier calipers, tape measures, and other tools to choose green forage maize with similar appearance and size for testing. Additionally, the moisture content of the material is measured as 65–75%.

### 2.5. Experimental Design and Statistical Analysis by RSM

Many factors affect the specific energy consumption and loss rate of header operation. In fact, during the harvest, the operator usually controls the forward speed of the harvester and the cutting height based on their own experience, which can easily lead to broken stalks and harvest loss. The uncut stalk is likely to wrap around the header, resulting in blockage and increased energy consumption. The number of stalk planting rows directly determines the planting density, which affects the harvest quality and effect of the header. The more rows, the more stalks cut and fed by the header, and the specific energy consumption of the header increases. Additionally, the interaction between stalks increases, which affects the feeding of stalks, is prone to blockage, and increases the loss rate of the header. Thus, this study selected the forward speed, cutting height, and number of rows as experimental factors. According to the forward speed range of the material conveyor (0–2.5 km/h) and the adjustment clearance range of the stalk fixing device, the forward speed is finally determined to be 1.0–2.0 km/h, and the number of rows is set at 2–4. Furthermore, the optimal stubble height for green forage maize is generally 100–200 mm. Hence, the cutting height is set at 100–200 mm. Experimental factors and levels are shown in Table 2.

**Table 2.** Experimental factors and levels.

Independent Variables	Coded	Range and Levels (Coded)		
		−1	0	+1
Forward speed (km/h)	$X_1$	1.2	1.6	2.0
Cutting height (mm)	$X_2$	100	150	200
Number of rows	$X_3$	2	3	4

This study selects the specific energy consumption and loss rate as the performance indexes of the header, and the calculation method is thus:

(1) Specific energy consumption

In the experiment, the test control can obtain the data of the torque and speed generated in the harvesting process. Then the specific energy consumption of header is calculated with Equation (1).

$$Y_1 = \frac{E_t - E_0}{M} \tag{1}$$

where  $E_t$  is the total specific energy consumption (kWh/t);  $E_0$  is the no-load specific energy consumption (kWh/t);  $M$  is the total mass of the test samples (t).

(2) Loss rate

The loss rate refers to the percentage of the mass of crops that are not cut or successfully fed into the header to the total mass of all tested crops in this group, which can be obtained from Equation (2).

$$Y_2 = \frac{M - m}{M} \times 100\% \tag{2}$$

where  $m$  is the total mass of the lost sample, (t).

The Box–Behnken design (BBD) method was used for experimental design (Table 3), and the obtained BBD data were analyzed and modeled based on the RSM statistical method (Equation (3)). In order to verify the accuracy of the RSM model and judge the significance of each factor in the RSM model, analysis of variance (ANOVA) was performed. In addition, three-dimensional response surface plots were drawn to explore the influence of various factors and their interactions on header performance.

$$Y = \beta_0 + \sum_{i=1}^n \beta_i X_i + \sum_{i < j} \beta_{ij} X_i X_j + \sum_{i=1}^n \beta_{ii} X_i^2, \tag{3}$$

where  $Y$  is the output response;  $X_i$  and  $X_j$  are the input variables;  $\beta_0$ ,  $\beta_i$ ,  $\beta_{ii}$ , and  $\beta_{ij}$  are the regression coefficients of the constant term, primary term, quadratic term, and interaction term of the equation, respectively.

**Table 3.** The Box-Behnken design scheme and results.

Run	Forward Speed $X_1$ /(km/h)	Cutting Height $X_2$ /(mm)	Number of Rows $X_3$	Specific Energy Consumption $Y_1$ /(kWh/t)	Loss Rate $Y_2$ /(%)
1	−1	1	0	0.232	1.34
2	0	1	1	0.171	0.71
3	−1	0	1	0.193	0.3
4	0	0	0	0.199	1.29
5	1	0	−1	0.246	2.02
6	−1	−1	0	0.274	1.76
7	1	−1	0	0.189	2.87
8	0	0	0	0.204	1.08
9	1	1	0	0.159	2.52
10	1	0	1	0.153	0.62
11	0	1	−1	0.231	2.36
12	0	0	0	0.213	1.13
13	0	−1	−1	0.303	2.45
14	−1	0	−1	0.341	1.27
15	0	−1	1	0.186	1.77
16	0	0	0	0.195	1.31
17	0	0	0	0.215	1.42

## 2.6. Artificial Neural Network (ANN)

Artificial neural networks (ANNs) are a widely applied mathematical and computational modeling method, which can be used to solve various problems in the field of science and engineering [32,33]. In this study, the BBD design data along with output response data are applied to establish and develop a multi-layer feed-forward neural network, which is used to predict the nonlinear relationship between the forward speed, cutting height, and number of rows and the specific energy consumption and loss rate of the header. With the connection weights and biases, the connections between neurons of each layer are established. Then, the data are transferred to each neuron via the transfer function. Finally, the output response is obtained [23]. In addition, during the training process, the weights and biases of the output layer to the hidden layer and the weights and biases of the hidden layer to the input layer are adjusted to minimize the error between the predicted value and the actual value [32], so as to establish the neural network model. This network consists of an input layer containing three input variables (forward speed, cutting height, and number of rows), a hidden layer containing several neuron numbers, and an output layer containing two output variables (specific energy consumption and loss rate). Its structure is shown in Figure 3.

Notably, the transfer function and the number of hidden layer neurons are key factors affecting the performance of neural networks [34]. Hence, it is necessary to determine the optimal combination of transfer functions and the number of hidden layer neurons in order to improve the reliability and accuracy of the neural network. Typically, there are three transfer functions, namely, the logistic sigmoid function (logsig), the hyperbolic tangent sigmoid function (tansig), and the linear transfer function (purelin). These are defined by expressions (4)–(6), respectively.

$$\log \text{sig}(n) = \left( \frac{1}{1 + e^{-n}} \right), \quad (4)$$

$$\tan \text{sig}(n) = \frac{1 - e^{-2n}}{1 + e^{-2n}}, \quad (5)$$

$$\text{purelin}(n) = n, \tag{6}$$

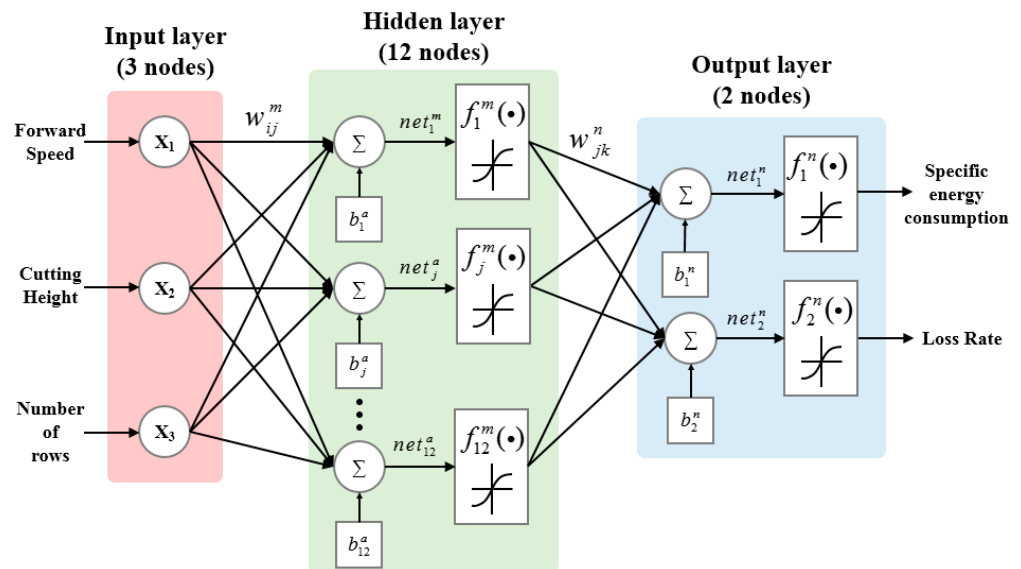


Figure 3. Structure of artificial neural network model.

In order to select the optimal combination of transfer functions, we studied the various combinations of the transfer function listed in Table 4. Furthermore, the optimal number of neurons is determined by trial and error method to obtain the optimal topology [35]. Consistent with other studies [22,34], the number of hidden layer neurons in this study ranges from 1 to 20.

Table 4. Comparison of different transfer function.

No.	Transfer Function		Mean Squared Error (MSE)	Determination Coefficient (R <sup>2</sup> )
	Hidden Layer	Output Layer		
1	tansig	purelin	0.01904	0.9365
2	tansig	tansig	0.002770	0.9908
3	logsig	purelin	0.005388	0.9820
4	logsig	tansig	0.003139	0.9895
5	purelin	purelin	0.08267	0.7243
6	purelin	tansig	0.07913	0.7361

The data obtained from the results of RSM are randomly divided into three parts, of which 11 groups (about 70%) are used for training, three groups (15%) are used for validation, and the remaining three groups (15%) are used for testing. Before training, the input and output parameters are normalized in the range of  $-1$  to  $+1$  (see Equation (7)) to reduce the impact of large difference between input and output parameters on training performance.

$$X_i = \frac{2}{d_{\max} - d_{\min}}(d_i - d_{\min}) - 1, \tag{7}$$

To evaluate the best training performance of the ANN model, this study employs the lowest root mean square error (RMSE), mean square error (MSE), and the highest determination coefficient (R<sup>2</sup>), the definitions of which are the same as those introduced in previous studies [30,36,37].

### 3. Results and Discussion

#### 3.1. RSM Modeling and Analysis

Response surface methodology is a mathematical and statistical tool widely used for analysis and prediction. In this study, RSM was used to explore the relationship between the three independent variables (forward speed, cutting height, and number of rows) and the two responses (specific energy consumption and loss rate). The regression analysis was conducted using design-Expert 8.0.6.1 software, and the regression model among the specific energy consumption and loss rate of the header and the three factors was obtained as shown in Equations (8) and (9).

$$Y_1 = 1.206 - 0.405X_1 - 1.36 \times 10^{-3}X_2 - 0.262X_3 + 1.5 \times 10^{-4}X_1X_2 + 0.0344X_1X_3 + 2.85 \times 10^{-4}X_2X_3 + 0.0588X_1^2 - 4.4 \times 10^{-7}X_2^2 + 0.0187X_3^2 \quad (8)$$

$$Y_2 = 4.827 + 0.660X_1 - 0.090X_2 + 2.051X_3 + 8.75 \times 10^{-4}X_1X_2 - 0.269X_1X_3 - 4.85 \times 10^{-3}X_2X_3 + 0.333X_1^2 + 3.29 \times 10^{-4}X_2^2 - 0.247X_3^2 \quad (9)$$

##### 3.1.1. Analysis of Variance (ANOVA)

As shown in Table 5, ANOVA was carried out to assess the adequacy and validity of the above models. For ANOVA, the F-value and p-value are typically used to confirm the statistical significance of the model [38]. From Table 5, it can be seen that the F-values of the specific energy consumption and loss rate are 33.66 and 22.03, and the p-values are all less than 0.001, demonstrating the reliability of both models. In addition, the F-values of 'Lack of fit' in these models are 2.69 and 3.52, respectively, which means that the developed RSM models are effective. The determination coefficients ( $R^2$ ) of the responses are 0.9625 and 0.9744, respectively, meaning that the predicted value of this model is very similar to the actual value and that the models have high statistical significance. According to the ANOVA, these three factors are found to have a significant impact on the specific energy consumption and loss rate. Among them, the number of rows has the greatest influence and the cutting height has the least.

**Table 5.** ANOVA for the experimental results of Box-Behnken design.

Source	Specific Energy Consumption (kWh/t)		Loss Rate (%)	
	F-Value	p-Value	F-Value	p-Value
Model	33.66	<0.0001 **	22.03	0.0002 **
X <sub>1</sub>	82.82	<0.0001 **	35.08	0.0006 **
X <sub>2</sub>	24.39	0.0017 **	11.45	0.0117 *
X <sub>3</sub>	168.55	<0.0001 **	68.63	<0.0001 **
X <sub>1</sub> X <sub>2</sub>	0.2778	0.6144	0.0304	0.8664
X <sub>1</sub> X <sub>3</sub>	5.84	0.0464 *	1.15	0.3193
X <sub>2</sub> X <sub>3</sub>	6.27	0.0408 *	5.85	0.0462 *
X <sub>1</sub> <sup>2</sup>	2.87	0.1340	0.2968	0.6028
X <sub>2</sub> <sup>2</sup>	0.0393	0.8485	70.93	<0.0001 **
X <sub>3</sub> <sup>2</sup>	11.30	0.0121 *	6.37	0.0396 *
Lack of fit	2.69	0.1818	3.52	0.1277

Note: p < 0.01 (Extremely significant, \*\*), p < 0.05 (Significant, \*).

##### 3.1.2. Analysis of Response Surface

The three-dimensional response surface plots between the output responses and three factors (one of which is fixed at the zero level) are drawn to visualize the influence of various factors and their interaction on the operation performance of the header [39].

Figure 4 shows the RSM plots of specific energy consumption. From Figure 4a, it can be seen that the specific energy consumption decreases gradually with the increase of the forward speed when the number of rows is three and the cutting height is constant. Likewise, the specific energy consumption of the header decreases with the increase of the cutting height as the forward speed is constant. This can be attributed to the fact that the larger the diameter of the stalk closer to the ground, the greater the cutting force required. If the forward speed is 2 km/h and the cutting height is 200 mm, the cutting time is short

and the cutting resistance is small. In this case, the specific energy consumption of the header is less than 0.18 kWh/t, which is at the lowest level. Conversely, the time and energy required to complete the operation is large, because the forward speed and cutting height are low. In addition, the forward speed contribution to the specific energy consumption is greater than the cutting height within the variation range of the test factors. That is to say, the forward speed has a greater impact on the specific energy consumption than that of the cutting height, which is consistent with the results of ANOVA (Table 3). As can be seen from Figure 4b,c, the specific energy consumption decreases significantly with the increase in the number of rows. This may be due to the impact of the number of rows on its cutting energy consumption, which is not obvious at the constant forward speed and cutting height. However, the more rows of stalks there are, the greater the total mass of stalks, leading to a reduction in specific energy consumption.

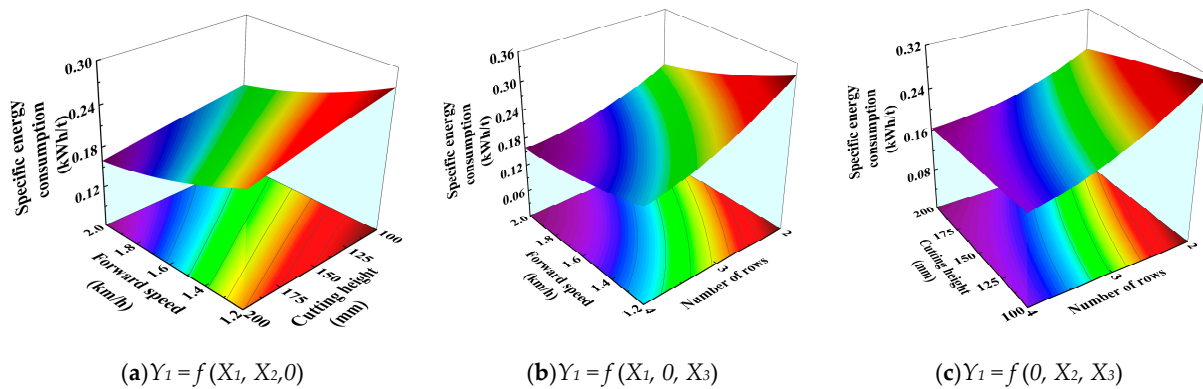


Figure 4. The interaction effects of variables on specific energy consumption of the header.

Figure 5 shows the response surface of various factors to the loss rate of the header. It can be observed from Figure 5a that when the cutting height is constant, the loss rate of the header gradually rises with the increase of the forward speed, which is the opposite of Figure 4a. This is due to the forward speed being too large, so the stalks do not cut smoothly and break. As the forward speed is constant, the loss rate first decreases and then increases with the increase of the cutting height. This may be because when the cutting height is high, the straw is easy to bend, resulting in the stalk breaking. If the cutting height is too low, the root of the stalk is easily damaged (soil loosens during field operations), which leads to the stalk not being cut and thus the stalk lodging in the field. From Figure 5a, it can be found that the loss rate is the highest for the condition of the forward speed of 2 km/h and the cutting height of 100 mm. This is because a higher speed has more impact force, damaging the root of the stalks and preventing them from being cut and fed to the header. From Figure 5b,c, the loss rate increases gradually with the increase of the number of rows.

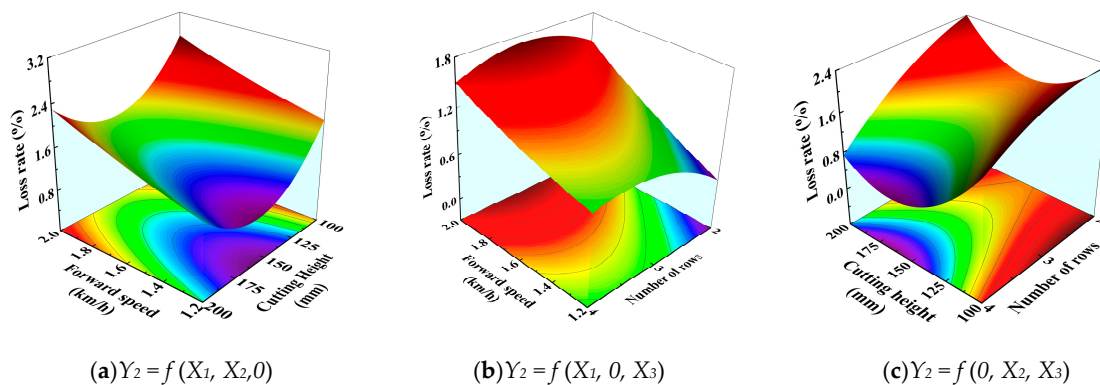


Figure 5. The interaction effects of variables on loss rate of the header.

### 3.1.3. Optimization

In order to optimize the harvester performance of the GFM harvester, based on BBD data and statistical analysis, this study used the desirability function method to numerically optimize the two responses, so as to obtain the best level of forward speed, cutting height and row number, and minimize the specific energy consumption and loss of the header [40]. The optimization method was proposed by Derringer and Suich [41] and is widely used in the optimization of multi-response processes in industry. The optimization criteria are shown in Table 6.

**Table 6.** Optimization criteria.

Name	Goal	Lower Limit	Upper Limit	Weight		Importance	Desirability
				Lower	Upper		
Forward speed	In range	1.20	2.00	1	1	3	1
Cutting height	In range	100	200	1	1	3	1
Number of rows	In range	2	4	1	1	3	1
Specific energy consumption	minimize	0.153	0.341	1	0.1	3	0.990928
Loss rate	minimize	0.300	2.87	1	0.1	3	0.998215

The optimization results show that the optimal parameter combination consists of the forward speed of 1.602 km/h, the cutting height of 167.4 mm, and the number of rows of 4. At this time, the specific energy consumption and loss rate are 0.1694 kWh/t and 0.3455%, respectively. However, in order to facilitate practical operation, the value of the optimal test factor is adjusted as follows: forward speed 1.6 km/h, cutting height 167 mm, and number of rows 4. To verify the accuracy of the optimization results, a validation test was carried out under the optimal conditions. The actual values of specific energy consumption and loss rate were 0.1701 kWh/t and 0.3466%, respectively, and the predicted values were 0.1696 kWh/t and 0.3429%, respectively, which were in good agreement with the observed values. The above results verified that the developed RSM model could be effectively used to study or optimize the header performance.

### 3.2. ANN Modeling and Analysis

A three-layer feed-forward neural network is developed to predict the performance of the header by applying the experimental data obtained by RSM. The neural network consists of an input layer, a hidden layer, and an output layer, as shown in Figure 3. Among them, the data of the input layer and the output layer are from Table 2. In order to determine the optimal transfer function combination of the artificial neural network, the transfer functions of the hidden and output layers are changed to carry out network training. The scheme is listed in Table 3. From Table 3, it can be found that the MSE of the network is the smallest and  $R^2$  is the largest when the transfer functions of both the hidden layer and the output layer are hyperbolic tangent sigmoid functions, which is consistent with the research of Aung et al. [42], Aydin et al. [32]. Therefore, the tansig function is selected as the transfer function of the ANN in this study. In addition, the performance of ANN with different topologies is evaluated by changing the number of the hidden layer neurons. Figure 6 shows that as the number of hidden layer neurons is 12, the performance of the ANN is best with the lowest mean square error (MSE) and the highest determination coefficient ( $R^2$ ) [36,43]. Hence, the optimal topology of the ANN is determined as 3-12-2.

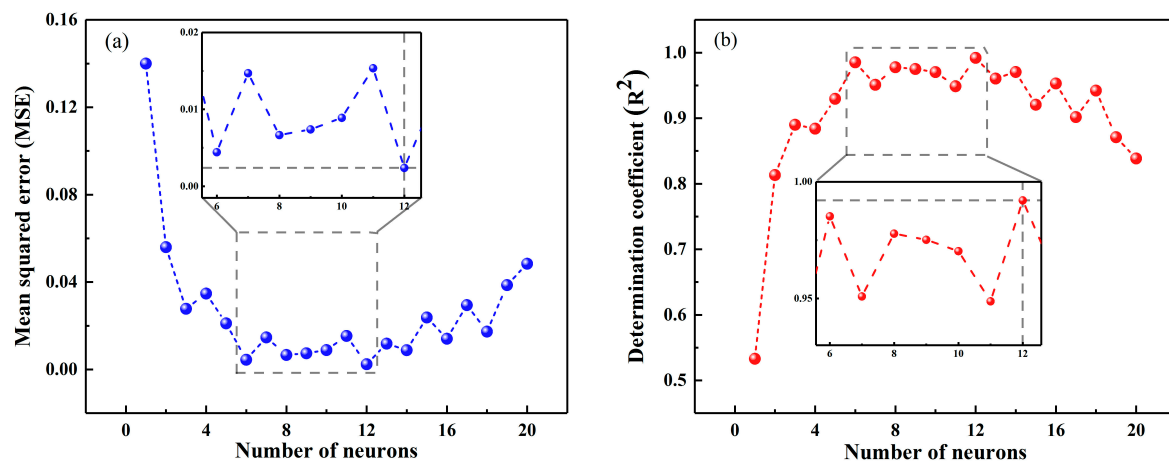


**Figure 6.** Determination of optimal number of neurons for ANN base on (a) MSE and (b)  $R^2$ .

The correlation coefficients ( $R$ ) of training, validation, and testing are 0.99719, 0.99115, and 0.99736, respectively, while the  $R$  of all data is 0.99602, as shown in Figure 7. It can be observed that the  $R$  of the ANN at all stages is close to 1.0, which means that the neural network model is reliable and efficient in predicting header performance. In addition, the MSE value of the neural network is 0.00313, indicating that the error between the predicted value and the actual value is minimal, that is to say, the neural network is accurate in predicting the output response. In summary, the RSM–ANN model developed in this study is viable in predicting the specific energy consumption and loss rate of the header.

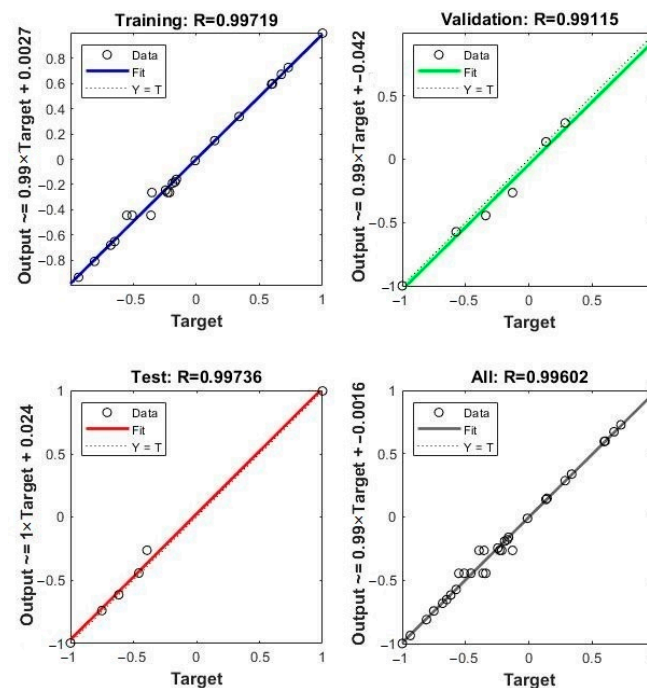


**Figure 7.** Regression plots of all stages and all datasets of ANN.

### 3.3. Comparison to the Traditional RSM

The values of  $R^2$ , MSE, and RMSE presented in Table 7 are used to assess the predictive capability of the RSM and RSM–ANN. Most studies used the same method [30,32]. The results demonstrate that the two models are effective in predicting the specific energy consumption and loss rate of the header. The  $R^2$  values of RSM and RSM–ANN models are greater than 0.95, which means that the predicted data is in good agreement with the

experimental data. In addition, from the higher  $R^2$  values of RSM–ANN than RSM, it indicates that the RSM–ANN has better prediction capability than RSM.

**Table 7.** Compare of RSM and RSM–ANN.

Statistical Parameters	Specific Energy Consumption (kWh/t)		Loss Rate (%)	
	RSM	RSM–ANN	RSM	RSM–ANN
$R^2$	0.9774	0.9925	0.9658	0.9906
MSE	0.00005341	0.00001775	0.01662	0.004558
RMSE	0.007308	0.004214	0.1289	0.06752

Figure 8 describes the relationship between the experimental values of specific energy consumption and loss rate and the predicted values of RSM–ANN and RSM models, respectively. As can be seen from Figure 8, the predicted values of the RSM–ANN are closer to the experimental values. Moreover, compared with the RSM model, the RSM–ANN model used to predict the specific energy consumption and loss rate has higher values of  $R^2$  and lower values of MSE and RMSE. The results indicate that the predicted values of the RSM–ANN agree well with the experimental data. In addition, the lower the error, the higher the precision and accuracy of the model.

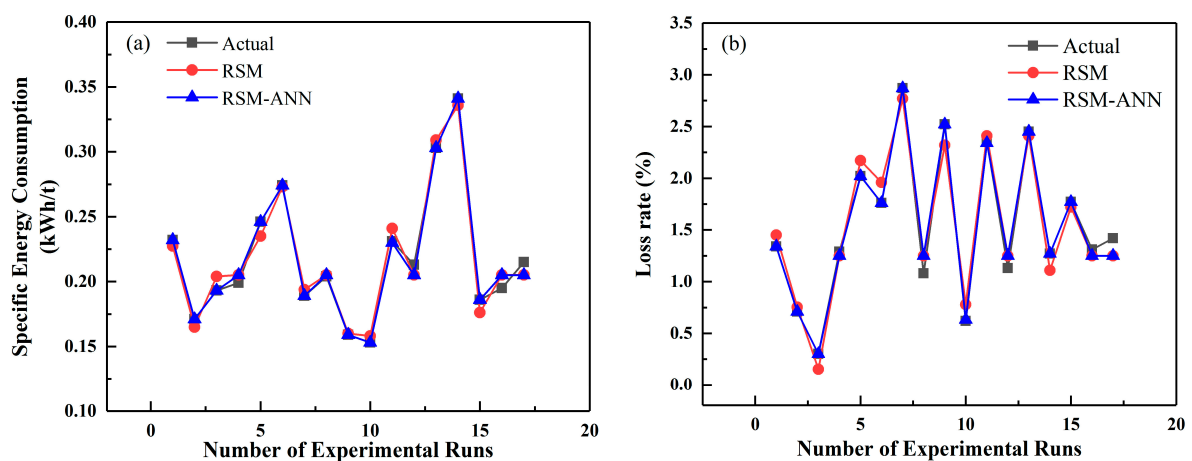


**Figure 8.** Comparison of the RSM and RSM- ANN predictions with the experimental values of (a) specific energy consumption and (b) loss rate.

In conclusion, the RSM–ANN is superior to the RSM in modeling and prediction performance. This finding is consistent with the conclusions of other researchers [37,44]. Of course, the RSM method has its own advantages. It can obtain a quadratic regression equation and show the influence of various factors and their interactions on the test index [45,46]. Hence, the combined RSM–ANN method is of great significance for the design, modeling, optimization, and performance prediction of agricultural machinery and equipment.

#### 4. Conclusions

In this study, a combined RSM–ANN approach was proposed, and the effects of forward speed, cutting height and row number on specific energy consumption and loss rate were studied. The main conclusions are as follows:

The optimal combination parameters are forward speed of 1.6 km/h, cutting height of 167 mm, and number of rows of 4. In addition, based on the experimental data obtained from RSM, the RSM–ANN model was established to predict the response, and the prediction ability of RSM and RSM–ANN was compared.  $R^2$  values of RSM and RSM–ANN are both greater than 0.95, indicating that both models have good predictive ability.

However, compared to RSM, RSM–ANN has better precision and accuracy in predicting header performance due to larger  $R^2$  and lower RMSE and MSE. In this case, the  $R^2$  of the RSM–ANN model for specific energy consumption and loss rate is 0.9925 and 0.9906, MSE is 0.00001775 and 0.004558, and RMSE is 0.004214 and 0.006752, respectively. In short, the combined RSM–ANN method can better predict and optimize header performance. This study can provide data and method references for the design and optimization of agricultural machinery, prediction and intelligent fault diagnosis of the operation parameters of harvesters.

**Author Contributions:** Z.X.: Conceptualization, Methodology, Data curation, Writing—original draft. J.F.: Conceptualization, Methodology, Writing—review & editing. Q.F.: Conceptualization, Writing—Review & editing, Funding acquisition, Formal analysis. X.L.: Resources, Software, Project administration; Z.C.: Formal analysis, Project administration. All authors have read and agreed to the published version of the manuscript.

**Funding:** The research presented in this article was supported by the National Key R&D Program of China (2022YFD2002102) and the National Natural Science Foundation of China (Grant No. 52105257).

**Institutional Review Board Statement:** Not applicable.

**Informed Consent Statement:** Not applicable.

**Data Availability Statement:** Not applicable.

**Acknowledgments:** Thanks to Gansu Academy of Mechanical Sciences Co., Ltd. for providing experimental materials and sites.

**Conflicts of Interest:** The authors declare that they have no known competing financial interests or personal relationships that could have appeared to influence the work reported in this paper.

## References

- Gao, Z.; Wang, W.; Lu, X.; Zhu, F.; Liu, W.; Wang, X.; Lei, C. Bioconversion performance and life table of black soldier fly (*Hermetia illucens*) on fermented maize straw. *J. Clean. Prod.* **2019**, *230*, 974–980. [CrossRef]
- FAOSTAT. Available online: <https://www.fao.org/faostat/en/#data/QCL> (accessed on 24 March 2023).
- Igathinathane, C.; Womac, A.R.; Sokhansanj, S. Corn stalk orientation effect on mechanical cutting. *Biosyst. Eng.* **2010**, *107*, 97–106. [CrossRef]
- Sun, M.; Xu, X.; Wang, C.; Bai, Y.; Fu, C.; Zhang, L.; Fu, R.; Wang, Y. Environmental burdens of the comprehensive utilization of straw: Wheat straw utilization from a life-cycle perspective. *J. Clean. Prod.* **2020**, *259*, 120702. [CrossRef]
- Ni, H.; Han, Y.; Cao, J.; Chen, L.W.A.; Tian, J.; Wang, X.; Chow, J.C.; Watson, J.G.; Wang, Q.; Wang, P.; et al. Emission characteristics of carbonaceous particles and trace gases from open burning of crop residues in China. *Atmos. Environ.* **2015**, *123*, 399–406. [CrossRef]
- Cai, Y.F.; Zheng, Z.H.; Schafer, F.; Stinner, W.; Yuan, X.F.; Wang, H.L.; Cui, Z.J.; Wang, X.F. A review about pretreatment of lignocellulosic biomass in anaerobic digestion: Achievement and challenge in Germany and China. *J. Clean. Prod.* **2021**, *299*, 16885. [CrossRef]
- Zhou, W.; Pian, R.Q.; Yang, F.Y.; Chen, X.Y.; Zhang, Q. The sustainable mitigation of ruminal methane and carbon dioxide emissions by co-ensiling corn stalk with *Neolamarckia cadamba* leaves for cleaner livestock production. *J. Clean. Prod.* **2021**, *311*, 127680. [CrossRef]
- Balafoutis, A.; Beck, B.; Fountas, S.; Vangeyte, J.; Van Der Wal, T.; Soto, I.; Gomez-Barbero, M.; Barnes, A.; Eory, V. Precision agriculture technologies positively contributing to ghg emissions mitigation, farm productivity and economics. *Sustainability* **2017**, *9*, 1339. [CrossRef]
- Mantoam, E.J.; Angnes, G.; Mekonnen, M.M.; Romanelli, T.L. Energy, carbon and water footprints on agricultural machinery. *Biosyst. Eng.* **2020**, *198*, 304–322. [CrossRef]
- Lisowski, A.; Klonowski, J.; Sypula, M.; Chlebowski, J.; Kostyra, K.; Nowakowski, T.; Struzyk, A.; Swietochowski, A.; Dabrowska, M.; Mieszkalski, L.; et al. Energy of feeding and chopping of biomass processing in the working units of forage harvester and energy balance of methane production from selected energy plants species. *Biomass Bioenergy* **2022**, *128*, 105301. [CrossRef]
- Li, Q.J.; Liang, R.Q.; Zhang, C.Y.; Ren, D.M.; Cheng, Y.T.; Zhang, D.X. Design of 4QG-2 silage harvester. *J. Agric. Mech. Res.* **2017**, *9*, 129–133. [CrossRef]
- Li, Q.J.; Zhong, B.; Ming, L.Q.; Sun, Z.M.; Zhang, D.X.; Gao, Q. Design of cutting conveying mechanism of the harvesting header of 4QZ-45 silage machine. *J. Agric. Mech. Res.* **2021**, *5*, 41–46. [CrossRef]

13. Ige, M.T.; Finner, M.F. Particle movement through the cutterhead of a cylindrical type forage harvester. *Trans. ASAE* **1975**, *18*, 1017–1020. [[CrossRef](#)]
14. McRandal, D.M.; McNulty, P.B. Impact cutting behaviour of forage crops I. Mathematical models and laboratory tests. *J. Agric. Eng. Res.* **1978**, *23*, 313–328. [[CrossRef](#)]
15. O'Dogherty, M.J. A review of research on forage chopping. *J. Agric. Eng. Res.* **1982**, *27*, 267–289. [[CrossRef](#)]
16. Chen, L.D.; Tian, K.Q.; Li, X.Y.; Du, F.B.; Zhang, C.L.; Xie, H. Structural design and mechanical analysis of the cutter of straw feed harvester. *J. Chinese Agric. Mech.* **2019**, *40*, 1–4+10. [[CrossRef](#)]
17. Tian, K.Q. Structure Design and Performance Test of 4.5 m Cutting Table of Self-Propelled Straw Feed Harvester. Master's Dissertation, Hebei Normal University of Science & Technology, Qinhuangdao, China, 2019.
18. Wang, J.H. Feeding Mechanism Research of Mower Table for Self-Propelled Silage Harvester. Master's Dissertation, Chinese Academy of Agricultural Mechanization Sciences, Beijing, China, 2011.
19. Liu, X.; Hou, J.L.; Li, W.; Feng, W.C.; Liu, J.G. Design on header of green fodder harvester. *J. Chin. Agric. Mech.* **2018**, *38*, 11–15. [[CrossRef](#)]
20. Gadekar, M.R.; Ahammed, M.M. Modelling dye removal by adsorption onto water treatment residuals using combined response surface methodology-artificial neural network approach. *J. Environ. Manag.* **2019**, *231*, 241–248. [[CrossRef](#)] [[PubMed](#)]
21. Suresh, T.; Sivrajasekar, N.; Balasubramani, K. Enhanced ultrasonic assisted biodiesel production from meat industry waste (pig tallow) using green copper oxide nanocatalyst: Comparison of response surface and neural network modelling. *Renew. Energy* **2021**, *164*, 897–907. [[CrossRef](#)]
22. Taoufik, N.; Boumya, W.; Elmoubarki, R.; Elhalil, A.; Achak, M.; Abdennouri, M.; Barka, N. Experimental design, machine learning approaches for the optimization and modeling of caffeine adsorption. *Mater. Today Chem.* **2022**, *23*, 100732. [[CrossRef](#)]
23. Singh, K.P.; Singh, A.K.; Gupta, S.; Rai, P. Modeling and optimization of reductive degradation of chloramphenicol in aqueous solution by zero-valent bimetallic nanoparticles. *Environ. Sci. Pollut. Res.* **2012**, *19*, 2063–2078. [[CrossRef](#)]
24. Raj, J.V.A.; Kumar, R.P.; Vijayakumar, B.; Gnansounou, E.; Bharathiraja, B. Modelling and process optimization for biodiesel production from *Nannochloropsis salina* using artificial neural network. *Bioresour. Technol.* **2021**, *329*, 124872. [[CrossRef](#)]
25. Tao, Y.; Wu, D.; Zhang, Q.A.; Sun, D.W. Ultrasound-assisted extraction of phenolics from wine lees: Modeling, optimization and stability of extracts during storage. *Ultrason. Sonochem.* **2014**, *21*, 706–715. [[CrossRef](#)] [[PubMed](#)]
26. Saldaña-Robles, A.L.; Bustos-Gaytán, A.; Diosdado-De la Peña, J.A.; Saldaña-Robles, A.; Alcántar-Camarena, V.; Balvantín-García, A.; Saldaña-Robles, N. Structural design of an agricultural backhoe using TA, FEA, RSM and ANN. *Comput. Electron. Agric.* **2020**, *172*, 105278. [[CrossRef](#)]
27. Srikanth, V.; Rajesh, G.K.; Kothakota, A.; Pandiselvam, R.; Sagarika, N.; Manikantan, M.R.; Sudheer, K.P. Modeling and optimization of developed cocoa beans extractor parameters using box-behnken design and artificial neural network. *Comput. Electron. Agric.* **2020**, *177*, 105715. [[CrossRef](#)]
28. Zeng, Z.H.; Chen, M.; Wang, X.M.; Wu, W.B.; Zheng, Z.F.; Hu, Z.B.; Ma, B.Q. Modeling and Optimization for Konjac Vacuum Drying Based on Response Surface Methodology (RSM) and Artificial Neural Network (ANN). *Processes* **2020**, *8*, 1430. [[CrossRef](#)]
29. Esonye, C.; Onukwuli, O.D.; Ofoefule, A.U. Optimization of methyl ester production from *Prunus Amygdalus* seed oil using response surface methodology and Artificial Neural Networks. *Renew. Energy* **2019**, *130*, 61–72. [[CrossRef](#)]
30. Yahya, H.S.M.; Abbas, T.; Amin, N.A.S. Optimization of hydrogen production via toluene steam reforming over Ni-Co supported modified-activated carbon using ANN coupled GA and RSM. *Int. J. Hydrog. Energy* **2021**, *46*, 24632–24651. [[CrossRef](#)]
31. Xue, Z.; Fu, J.; Chen, Z.; Wang, F.D.; Han, S.P.; Ren, L.Q. Optimization experiment on parameters of chopping device of forage maize harvester. *J. Jilin Univ. Eng. Technol. Ed.* **2020**, *50*, 739–748. [[CrossRef](#)]
32. Aydin, M.; Uslu, S.; Çelik, M.B. Performance and emission prediction of a compression ignition engine fueled with biodiesel-diesel blends: A combined application of ANN and RSM based optimization. *Fuel* **2020**, *269*, 117472. [[CrossRef](#)]
33. Hariharan, N.; Senthil, V.; Krishnamoorthi, M.; Karthic, S.V. Application of artificial neural network and response surface methodology for predicting and optimizing dual-fuel CI engine characteristics using hydrogen and bio fuel with water injection. *Fuel* **2020**, *270*, 117576. [[CrossRef](#)]
34. Talebian-Kiakalaieh, A.; Amin, N.A.S.; Zarei, A.; Noshadi, I. Transesterification of waste cooking oil by heteropoly acid (HPA) catalyst: Optimization and kinetic model. *Appl. Energy* **2013**, *102*, 283–292. [[CrossRef](#)]
35. Cemek, B.; Ünlükara, A.; Kurunç, A.; Küçüktopcu, E. Leaf area modeling of bell pepper (*Capsicum annuum* L.) grown under different stress conditions by soft computing approaches. *Comput. Electron. Agric.* **2020**, *174*, 105514. [[CrossRef](#)]
36. Ciric, A.; Krajnc, B.; Heath, D.; Ogrin, N. Response surface methodology and artificial neural network approach for the optimization of ultrasound-assisted extraction of polyphenols from garlic. *Food Chem. Toxicol.* **2020**, *135*, 110976. [[CrossRef](#)] [[PubMed](#)]
37. Onukwuli, D.O.; Esonye, C.; Ofoefule, A.U.; Eyisi, R. Comparative analysis of the application of artificial neural network-genetic algorithm and response surface methods-desirability function for predicting the optimal conditions for biodiesel synthesis from *Chrysothamnus albidum* seed oil. *J. Taiwan Inst. Chem. Eng.* **2021**, *125*, 153–167. [[CrossRef](#)]
38. Liu, Z.W.; Xiao, H.; Khatri, P.; Ding, S.L.; Wang, X. A study of a flux switching linear generator with a novel speed amplified mechanism and its optimization for the maximum power output and minimum cogging force of wave energy conversion. *Mech. Syst. Signal Process* **2022**, *166*, 108413. [[CrossRef](#)]

39. Chaker, H.; Ameer, N.; Saidi-Bendahou, K.; Djennas, M.; Fourmentin, S. Modeling and Box-Behnken design optimization of photocatalytic parameters for efficient removal of dye by lanthanum-doped mesoporous TiO<sub>2</sub>. *J. Environ. Chem. Eng.* **2021**, *9*, 104584. [[CrossRef](#)]
40. Yolmeh, M.; Jafari, S.M. Applications of response surface methodology in the food industry processes. *Food Bioprocess Technol.* **2017**, *10*, 413–433. [[CrossRef](#)]
41. Derringer, G.; Suich, R. Simultaneous optimization of several response variables. *J. Qual. Technol.* **1980**, *12*, 214–219. [[CrossRef](#)]
42. Aung, T.; Kim, S.-J.; Eun, J.-B. A hybrid RSM-ANN-GA approach on optimisation of extraction conditions for bioactive component-rich laver (*Porphyra dentata*) extract. *Food Chem.* **2022**, *366*, 130689. [[CrossRef](#)]
43. Sharafi, K.; Pirsahab, M.; Gupta, V.K.; Agarwal, S.; Moradi, M.; Vasseghian, Y.; Dragoi, E.N. Phenol adsorption on scoria stone as adsorbent- application of response surface method and artificial neural networks. *J. Mol. Liq.* **2019**, *274*, 699–714. [[CrossRef](#)]
44. Gupta, S.; Patel, P.; Mondal, P. Biofuels production from pine needles via pyrolysis: Process parameters modeling and optimization through combined RSM and ANN based approach. *Fuel* **2022**, *310*, 122230. [[CrossRef](#)]
45. Jiang, Q.J.; He, Z.L.; Wang, Y.W.; Wang, J. Optimizing the working performance of a boat-type tractor using central composite rotatable design and response surface method. *Comput. Electron. Agric.* **2021**, *181*, 105944. [[CrossRef](#)]
46. Santana, J.C.C.; Araújo, S.A.; Alves, W.A.L.; Belan, P.A.; Ling, J.G.; Chen, J.C.; Liu, D.H. Optimization of vacuum cooling treatment of postharvest broccoli using response surface methodology combined with genetic algorithm technique. *Comput. Electron. Agric.* **2018**, *144*, 209–215. [[CrossRef](#)]

**Disclaimer/Publisher’s Note:** The statements, opinions and data contained in all publications are solely those of the individual author(s) and contributor(s) and not of MDPI and/or the editor(s). MDPI and/or the editor(s) disclaim responsibility for any injury to people or property resulting from any ideas, methods, instructions or products referred to in the content.